International Journal of Mechanical, Industrial and Aerospace Sciences
ISSN: 2517-9950
Vol:11, No:1, 2017

Parametric Analysis and Optimal Design of Functionally Graded Plates Using Particle Swarm Optimization Algorithm and a Hybrid Meshless Method

Foad Nazari, Seyed Mahmood Hosseini, Mohammad Hossein Abolbashari, Mohammad Hassan Abolbashari

***Abstract*—**The present study is concerned with the optimal design of functionally graded plates using particle swarm optimization (PSO) algorithm. In this study, meshless local Petrov-Galerkin (MLPG) method is employed to obtain the functionally graded (FG) plate's natural frequencies. Effects of two parameters including thickness to height ratio and volume fraction index on the natural frequencies and total mass of plate are studied by using the MLPG results. Then the first natural frequency of the plate, for different conditions where MLPG data are not available, is predicted by an artificial neural network (ANN) approach which is trained by back-error propagation (BEP) technique. The ANN results show that the predicted data are in good agreement with the actual one. To maximize the first natural frequency and minimize the mass of FG plate simultaneously, the weighted sum optimization approach and PSO algorithm are used. However, the proposed optimization process of this study can provide the designers of FG plates with useful data.

***Keywords*—**Optimal design, natural frequency, FG plate, hybrid meshless method, MLPG method, ANN approach, particle swarm optimization.

I. Introduction

A new generation of materials including two or more phases with a smoothly varying composition of gradually changing of the volume fraction of the materials is called functionally graded materials (FGMs). This kind of composite materials have some improved properties in comparison to conventional composites. Some research works have been performed by focusing on the vibration of FGMs [1]-[3]. Also, Vel and Batra [4] have proposed a solution for free and forced vibrations of rectangular FG plates. In another study, Batra and Jin [5] investigated the FGM anisotropic plates with various boundary conditions by applying the finite element method and the first-order shear deformation theory. Ferreira et al. [6] and Roque et al. [7] presented a meshless method based on radial basis functions for free vibration of FG plates. Matsunaga [8] performed a dynamic and stability analysis of simply supported edges FGM plates using several sets of 2D advanced approximate theories. In another study, Iqbal et al. [9] investigated the vibration characteristics of FG cylindrical shells by wave propagation approach. An analytical method for dynamic response analysis of FG thick hollow cylinders under impact loading was presented by Hosseini and Abolbashari [10]. In their study, the wave motion equation was analytically solved by using the composition of Bessel functions. In another study, Asgari et al. [11] studied a thick hollow cylinder with finite length made of 2D-FGM and subjected to impact internal pressure. Najafizadeh and Isvandzibaei [12] presented a study on the vibration of thin cylindrical shells with ring supports made of FGMs composed of stainless steel and nickel, which was carried out based on third order shear deformation shell theory. Fallah et al. [13] studied free vibration analysis of moderately thick rectangular FG plates on elastic foundation with various combinations of simply supported and clamped boundary conditions based on the Mindlin plate theory. In another study, Aragh and Yas [14] investigated three-dimensional (3D) free vibration analysis of four-parameter continuous grading fiber reinforced cylindrical panels resting on Pasternak foundations by using generalized power-law distribution. Ebrahimi and Rastgoo [15] presented a theoretical model for geometrically nonlinear vibration analysis of thermo-piezoelectrically actuated circular FG plates based on Kirchhoff's–Love hypothesis with von-Karman type geometrical large nonlinear deformations. Furthermore, Allahverdizadeh et al. [16] studied the nonlinear vibration of a thin circular FG material plate using shooting and Runge–Kutta methods.

MLPG is the first monograph on new class of meshless methods that are expected to revolutionize engineering/science analyses. The MLPG method eliminates the intensive human-labor costs involved in an analysis. It is often computationally less-expensive, as compared to the Finite Element and Boundary Element Methods. Atluriet and Zhu [17], [19] and Atluriet et al. [18] developed the MLPG method which is based on the local weak instead of global weak formulation of the problem. Sladek et al. [20] presented a review study on the analysis of problems in engineering and the sciences using MLPG method. In another study, Sladek et al. [21] used MLPG method for 2D static and dynamic deformations of FG

Foad Nazari is now with Mechanical Engineering Department, Lean Production Engineering Research Center, Ferdowsi University of Mashhad, PO Box 91775-1111, Mashhad, Iran (e-mail: foadnazari@gmail.com).

Seyed Mahmoud Hosseini is now with Industrial Engineering Department, Ferdowsi University of Mashhad, PO Box 91775-1111, Mashhad, Iran (e-mail: sm_hoseini@yahoo.com).

Mohammad Hossein Abolbashari is now with Mechanical Engineering Department, Lean Production Engineering Research Center, Ferdowsi University of Mashhad, PO Box 91775-1111, Mashhad, Iran (phone: 98-51-38805004; fax: +98-51-38763304; e-mail: abolbash@um.ac.ir).

Mohammad Hassan Abolbashari is now with School of Business, UNSW Canberra, BC 2610, Australia.

solids. In two other studies, Qian et al. [22] and Gilhooley et al. [23] investigated the static and dynamic deformations of thick FGM plates by applying a higher-order shear and normal deformable plate theory and the MLPG method. RezaeiMojdehi et al. [24] presented the static and dynamic analysis of thick FG plates using MLPG method. Also, a hybrid technique based on composition of Newmark finite difference and MLPG methods was applied for natural frequencies analysis of a thick FG cylinder by Hosseini [25].

In the recent years, artificial intelligence techniques such as ANN and optimization algorithms have attracted the attention of many researchers in the different fields of study such as vibration of FG structures. For example, Kamarian et al. [26] applied ANN, genetic and imperialist competitive algorithm (ICA) for optimization of volume fraction of FG beams resting on elastic foundation for maximizing the first natural frequency. Furthermore, Jodaei et al. [27] used ANN technique for 3D analysis of FG annular plates by applying state-space based differential quadrature method. Jam et al. [28] also focused on free vibration characteristics of FG rectangular plates resting on Pasternak foundation based on the 3D elasticity theory and by means of the generalized differential quadrature method. They carried out a detailed parametric study to highlight the influences of different affecting parameters on the vibration characteristics of the FG plates. The main goal of their study was FG plate's density minimizing to achieve a specified fundamental frequency using ICA and ANN and presenting the optimized material profile.

In this study, PSO algorithm and a hybrid meshless method based on MLPG and ANN approach are used for the optimal design of FG plates to maximize the first natural frequency and minimize the mass of FG plate, simultaneously. The MLPG method is employed to obtain some data for training the ANN. The trained ANN can predict the first natural frequencies in various conditions. Finally, the PSO algorithm is used to maximize the first natural frequency and also to minimize the mass of FG plate.

II. Model Description

A rectangular FG plate with uniform thickness is considered in this study. Fig. 1 shows a schematic view of the plate in the Cartesian coordinates (x, y, z).

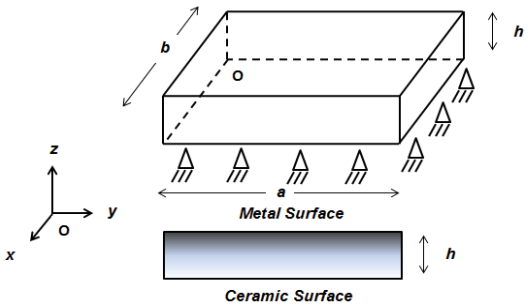

Fig. 1 Schematic of FG plate in rectangular Cartesian coordinate

A common pattern for describing the FG variation of material properties is power-law function. Also the elasticity modulus and density assumed to vary continuously due to gradually changing the volume fraction of the constituent materials. The Poisson's ratio is assumed to be constant and equal to 0.3. Along the thickness direction of the plate, volume fraction of material number 1 (bottom surface) is assumed to obey (1):

$$g(\mu) = \mu^{p} \tag{1}$$

where p stands for volume fraction index of power-law pattern and $\mu = z/h$. Also, volume fraction function at any height is denoted by g. The mixture rule is to express the effective material properties of the plate along the thickness consists of Young's modulus and mass density according to (2).

$$\eta_e(\mu) = \eta_b + (\eta_t - \eta_b) g(\mu). \tag{2}$$

where η_e denotes the effective material properties of FG plate. The terms η_b and η_c in (2) are the properties of the bottom and top surfaces, respectively.

III. Applying the MLPG Method for 3D Problems

Assume the problem of linear elasticity where the 3D equation of motion in the domain of Ω, which is bounded by the surface Γ, in absence of any body force, is as:

$$\sigma_{ij,j}(X,t) = \rho(X)\ddot{u}_i(X,t), \quad in \ \ \Omega \tag{3}$$

where the indices i and j take the values of 1, 2, and 3 and refer to Cartesian coordinates of x, y, and z, respectively. Also, $\sigma_{ij}(X,t)$, ρ and $\ddot{u}_i(X,t) = \partial^2 u_i(X,t)/\partial t^2$ are the stress tensor, density and acceleration field, respectively. The boundary conditions are assumed as:

$$\sigma_{ij}(X,t) n_j(X) = \bar{t}_i(X,t) \ on \ \ \Gamma_t \tag{4}$$

$$u_i(X,t) = \bar{u}_i(X,t) \ on \ \ \Gamma_u \tag{5}$$

where n_j, $u_i(X,t)$, and $t_i(X,t)$ represent the unit outward vector normal to boundary Γ_t, the displacement component and the surface traction components, respectively. Also $\bar{u}_i(X,t)$ and $\bar{t}_i(X,t)$ are the prescribed displacement and prescribed traction on Γ_u and Γ_t, respectively.

For a plate undergoing free vibration, its periodic displacement components can be illustrated in terms of the displacement amplitude functions, $u_i = U_i \exp(\bar{J}\omega t)$, where $\bar{J} = \sqrt{-1}$ and ω and U_i denote the natural frequency of the

plate and maximum amplitude of u_i, respectively.

As indicated in Fig. 2, brick-shaped local domains in this study are considered as sub-domains and support domains. Because the global domain of the rectangular plate is parallelepiped when the local sub-domain intersects the global boundary, the mapping procedure is simple, and no special treatment is needed.

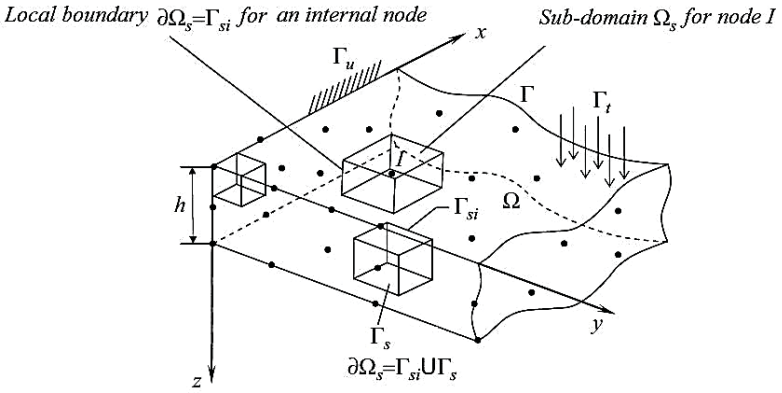

Fig. 2 Sub-domains and global domain for a rectangular plate

A. 3D Elastic Body Local Symmetric Weak Form

The generalized local weak form of the equilibrium equations over a local sub-domain around node i, can be written as:

$$\int_{\Omega_s^I}(\sigma_{ij,j}(X,t)+\omega^2\rho u_i(X,t))\lambda_I(X)d\Omega\partial - \xi\int_{\Gamma_{su}^I}(u_i(X,t)-\bar{u}_i(X,t))\lambda_I(X)d\Gamma=0 \tag{6}$$

As this paper deals with the free vibration analysis, the body force vector is assumed to be zero. In this equation $\lambda_I(X)$ and $u_i(X,t)$ are the test and trial functions, respectively. In (6), the term Γ_{su}^I is a part of the boundary Ω_s^I over which the essential boundary is prescribed. Also ξ is a penalty parameter to impose the essential boundary condition ξ £ 1. One can write:

$$\sigma_{ij,j}(X,t)\lambda_I=(\sigma_{ij}(X,t)\lambda_I)_{,j}-\sigma_{ij}(X,t)\lambda_{I,j} \tag{7}$$

Using the divergence theory and (7), (8) is obtained:

$$\begin{aligned}&\int_{\partial\Omega_s^I}\sigma_{ij}(X,t)n_j(X)\lambda_I(X)d\Gamma\\&-\int_{\Omega_s^I}(\sigma_{ij}(X,t)\lambda_{I,j}(X))d\Omega\\&-\xi\int_{\Gamma_{su}^I}(u_i(X,t)-\bar{u}_i(X,t))\lambda_I(X)d\Gamma\\&+\int_{\Omega_s^I}\omega^2\rho u_i(X,t)\lambda_I(X)d\Omega=0\end{aligned} \tag{8}$$

By substitution of $\bar{u}_i(X,t)=0$ in (8), (9) which is the symmetric local weak form of linear elastic free vibration is obtained.

$$\begin{aligned}&\int_{\Omega_s^I}\sigma_{ij}(X,t)\lambda_{I,j}(X)d\Omega-\int_{\Gamma_{su}^I}t_i(X,t)\lambda_I(X)d\Gamma\\&-\int_{\Gamma_{st}^I}t_i(X,t)\lambda_I(X)d\Gamma+\xi\int_{\Gamma_{su}^I}u_i(X,t)\lambda_I(X)d\Gamma\\&-\omega^2\int_{\Omega_s^I}\rho u_i(X,t)\lambda_I(X)d\Omega=0.\end{aligned} \tag{9}$$

In (9), Γ_{si}^I is a part of local boundary which is placed inside the global domain. It does not have any contact with the problems' global boundary. Furthermore, Γ_{st}^I and Γ_{su}^I are parts of the local boundary that coincide with the global traction and displacement boundaries, respectively. It should be mentioned that $\lambda_I(X)$ should be chosen such that to be vanished outside and positive inside the Ω_s. Consequently, Ω_s^I (the boundary of local sub-domain) consists of three parts, $\partial\Omega_s^I=\Gamma_{si}^I\cup\Gamma_{su}^I\cup\Gamma_{st}^I$.

B. MLS 3D Approximation

The unknown trial approximant $\tilde{u}(X)$ of $u(X)$ in Moving Least Square (MLS) approximation is as follow:

$$\begin{aligned}\tilde{u}(X)&=p^T(X)a(X)\quad\forall X\in\Omega_X;\ p^T(X)\\&=[p_1(X),p_2(X),p_3(X),...,p_m(X)]\end{aligned} \tag{10}$$

where $p^T(X)$ is a complete monomial basis of order m, which for 3D problems a quadratic basis vector can be defined as (11). Furthermore, the defined domain of MLS approximation at point X for the trial function is denoted by Ω_X.

$$p^T(X)=[1,x,y,z,x^2,y^2,z^2,xy,yz,zx]. \tag{11}$$

A weighted discrete L2-norm of equation is as follow:

$$J(a(X)) = \sum_{I=1}^{N} g_I(X)[p^T(X_I)a(X) - \hat{u}^I]^2 = [P.a(X) - \hat{u}]^T G(X)[P.a(X) - \hat{u}]. \quad (12)$$

By minimizing (12), the coefficient vector of $a(X)$ is determined. In (12), $g_I(X)$ is the weight function of node I. Also, it is strictly positive ($g_I(X) > 0$) for all points located in the support domain of weight function. Moreover, X_I is the I[th] node position, and $\hat{u}^I (I = 1,2,3,...,N \; \hat{I} \; \Omega_X)$ presents the fictitious nodal value. Furthermore, G , P and $\hat{u}$ are as:

$$P = \begin{bmatrix} p^T(X_1) \\ p^T(X_2) \\ . \\ . \\ . \\ p^T(X_N) \end{bmatrix}_{N \times m},$$

$$G = \begin{bmatrix} g_1(X) & 0 & . & . & . & 0 \\ 0 & . & & & & . \\ . & & . & & & . \\ . & & & . & & . \\ . & & & & . & 0 \\ 0 & . & . & . & 0 & g_N(X) \end{bmatrix}_{N \times N}, \quad (13)$$

$$\hat{u} = [\hat{u}_1, \hat{u}_2, ..., \hat{u}_N]_{1 \times N}$$

In this study, $\partial(.)/\partial X_i$ is denoted by $(.)_{,i}$. The approximation of $\tilde{u}(X)$ can be obtained by substitution of $a(X)$ in (10) as (14).

$$\tilde{u}(X) = \sum_{I=1}^{N} \phi^I(X)\hat{u}^I \quad (14)$$

Also, the partial derivatives of the trial function, $\tilde{u}_{,i}(X)$, and MLS approximation shape function, $f^I(X)$, and its derivative, $f^I_{,i}(X)$, are obtained as (15)-(17), respectively.

$$\tilde{u}_{,i}(X) = \sum_{I=1}^{N} \phi^I_{,i}(X)\hat{u}^I \quad (15)$$

$$\phi^I(X) = \sum_{j=1}^{m} p_j(X)[A^{-1}(X)B(X)]_{jI} \quad (16)$$

$$\phi^I_{,i}(X) = \sum_{j=1}^{m} [p_{j,i}(A^{-1}B)_{jI} + p_j(A^{-1}B_{,i} + A^{-1}_{,i}B)_{jI}] \quad (17)$$

Moreover, R_i is the support size of the weight function, defined as $R_i = \tau \bar{l}^I$ (18), where τ denotes the dimensionless size of cubic support domain.

$$R_x = \tau \bar{l}^I_x; \quad R_y = \tau \bar{l}^I_y; \quad R_z = \tau \bar{l}^I_z. \quad (18)$$

Furthermore, $\bar{l}$ denotes the average of nodal spacing in the vicinity of node I between two neighboring nodes in (19):

$$\bar{l}^I_x = |x - x_I|; \quad \bar{l}^I_y = |y - y_I|; \quad \bar{l}^I_z = |z - z_I|. \quad (19)$$

C. Heaviside Step Test Function

In this study, the test function assumed to be Heaviside step function which corresponds to MLPG5 (20):

$$\lambda(X) = \begin{cases} 1 & X \in \Omega_s \\ 0 & X \notin \Omega_s \end{cases} \quad (20)$$

In MLPG5 method, the local nodal-based test function, over a local sub-domain centered at a node, is the Heaviside step function. In numerical integration, a definite integral is approximated by evaluating the integral at a finite set of points called integration points and then a weighted sum of these values is used to provide an approximation. If Gaussian quadrature is used as a rule for the approximation, the integration points take specific locations and weights, thus an integration point becomes a Gauss point. By using this method, there is no need for both a domain integral in the attendant symmetric weak-form and a singular integral.

The sub-domain dimension for node I is defined as $(2\psi \bar{l}^I_x) \times (2\psi \bar{l}^I_y) \times (2\psi \bar{l}^I_z)$, where ψ is a constant between 0 and 1. For support of the test function, brick-shaped sub-domain is selected.

The discretized system of linear equations is obtained by substituting the MLS approximation function, (14) into (9) and summing up for all nodes, as:

$$\sum_{J=1}^{\tilde{S}} (\tilde{K}_{IJ} - \omega^2 \tilde{M}_{IJ})\hat{u}^J(X,t) = 0, \quad (21)$$

In this equation, $\tilde{S}$, $\tilde{K}$, and $\tilde{M}$ denote the total number of nodes, the stiffness and mass matrixes, respectively. Therefore, for the MLPG5 method, $\tilde{K}$ and $\tilde{M}$ are as:

$$\tilde{M}_{IJ} = \int_{\Omega^I_s} \rho \Phi^J d\Omega \quad (22)$$

$$\tilde{K}_{IJ} = -\int_{\Gamma_{si}^{I}} NDB^{J} d\Gamma - \int_{\Gamma_{su}^{I}} SNDB^{J} d\Gamma + \xi \int_{\Gamma_{su}^{I}} S\Phi^{J} d\Gamma \quad (23)$$

The vectors and matrices of (22) and (23) in 3D space are as (24)-(29). Also Poisson's ratio and Young's modulus are denoted by v and E, respectively. In this study, E and ρ are considered to vary through the thickness according to power-law model.

$$D=\frac{E(z)(1-v)}{(1-2v)(1+v)}\begin{bmatrix} 1 & \frac{v}{1-v} & \frac{v}{1-v} & 0 & 0 & 0 \\ \frac{v}{1-v} & 1 & \frac{v}{1-v} & 0 & 0 & 0 \\ \frac{v}{1-v} & \frac{v}{1-v} & 1 & 0 & 0 & 0 \\ 0 & 0 & 0 & \frac{1-2v}{2(1-v)} & 0 & 0 \\ 0 & 0 & 0 & 0 & \frac{1-2v}{2(1-v)} & 0 \\ 0 & 0 & 0 & 0 & 0 & \frac{1-2v}{2(1-v)} \end{bmatrix} \quad (24)$$

$$B^{J} = \begin{bmatrix} \phi^{J}_{,x} & 0 & 0 \\ 0 & \phi^{J}_{,y} & 0 \\ 0 & 0 & \phi^{J}_{,z} \\ \phi^{J}_{,y} & \phi^{J}_{,x} & 0 \\ 0 & \phi^{J}_{,z} & \phi^{J}_{,y} \\ \phi^{J}_{,z} & 0 & \phi^{J}_{,x} \end{bmatrix}, \quad (25)$$

$$\Phi^{J} = \begin{bmatrix} \phi^{J} & 0 & 0 \\ 0 & \phi^{J} & 0 \\ 0 & 0 & \phi^{J} \end{bmatrix}, \quad (26)$$

$$\hat{u}^{J} = \begin{Bmatrix} \hat{u}^{J}_{x} \\ \hat{u}^{J}_{y} \\ \hat{u}^{J}_{z} \end{Bmatrix}, \quad (27)$$

$$S = \begin{bmatrix} S_x & 0 & 0 \\ 0 & S_y & 0 \\ 0 & 0 & S_z \end{bmatrix};$$

$$S_k = \begin{Bmatrix} 1 & (u_k \text{ is prescribed on } \Gamma_u) \\ 0 & (u_k \text{ is not prescribed on } \Gamma_u) \end{Bmatrix}; \quad (28)$$

$$k = x, y, z$$

$$N = \begin{bmatrix} \tilde{n}_x & 0 & 0 & \tilde{n}_y & 0 & \tilde{n}_z \\ 0 & \tilde{n}_y & 0 & \tilde{n}_x & \tilde{n}_z & 0 \\ 0 & 0 & \tilde{n}_z & 0 & \tilde{n}_y & \tilde{n}_x \end{bmatrix}, \quad (29)$$

IV. Artificial Intelligence Approach for Prediction and Optimization

The proposed procedure of this study for optimization of FG plate is based on the PSO algorithm and a hybrid meshless method. The employed hybrid meshless method is based on MLPG and ANN approaches. In this approach, the MLPG method is used for obtaining the natural frequencies of FG plates for different plate thicknesses and volume fraction index values. The ANN is trained based on the MLPG results. Then, the trained ANN is used to predict the first natural frequency of the plate for some other plate thicknesses and volume fraction index values. Indeed, the trained ANN converts the discrete data to a continuous function, which can provide the first natural frequency of the plate for any plate thicknesses and volume fraction index values. As the next step, the PSO algorithm is applied for simultaneous optimization of plate mass and natural frequency. It is clear that the mass of the plate is desired to be minimized and the natural frequency be maximized. In this respect, since global minimization of mass and global maximization of first natural frequency do not necessarily occurs simultaneously, the weighted sum optimization approach is employed. The main idea in the weighted sum method is to choose a weighting coefficient for each objective functions. So, the multi-criteria optimization problem is transformed to a single-objective one. In this study, for different weighting coefficient values, the optimum plate thickness and volume fraction index values are obtained. The optimization procedure furnishes the designers with useful information which they need for FG plate.

A. Artificial Neural Network

ANNs are a form of a multi-processor system with a high degree of inter-connection simple processing elements, adoptive interaction between elements and simple scalar messages. The multi-layer feed forward (MLFF) is the most popular type of ANNs which is shown in Fig. 3.

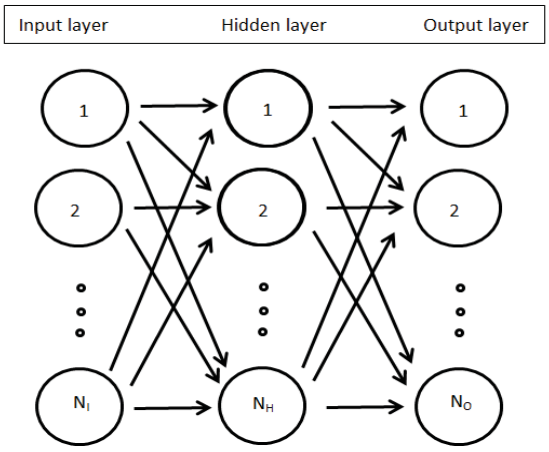

Fig. 3 A typical MLFF neural network

The MLFF network consists of an input layer, one or more hidden layers and an output layer which each layer includes some neurons. As can be seen in Fig. 3, number of neurons in

input, hidden, and output layers of ANN denoted with NI, NH, and NO, respectively. In this network, knowledge is stored in connection weights. In this study, an ANN is trained based on the most widely used learning algorithm of MLFF ANNs which called back error propagation (BEP) method [29]. For the prediction of first non-dimensional natural frequencies of FG plate, the inputs of the ANN are the volume fraction index and non-dimensional FG plate thickness, and corresponding non-dimensional first natural frequency is the target outputs. [8].

B. Back-Error Propagation

Repeating three BEP stages lead to a value of the error function, which will be zero or a constant value and so the designed ANN is trained.

The transfer function for the neurons of hidden and output layers of all ANNs is Tansig and is defined in (30).

$$TF(\bar{n}) = \frac{2}{\left(1+e^{-2\bar{n}}\right)} - 1 \tag{30}$$

The operation of the BEP method consists of three steps as:

1- Feed-forward stage:

$$\bar{T} = \bar{W}_{bc}(\bar{n}).\bar{Y}(\bar{n}), \tag{31}$$

$$\bar{O}(\bar{n}) = \bar{\Phi}\left(\bar{T}(\bar{n})\right) = \frac{2}{1+\mathrm{e}^{\bar{T}(2\bar{n})}} - 1, \tag{32}$$

where the output, input, output of hidden layer, and activation function are denoted with $\bar{O}, \bar{T}, \bar{Y}$ and $\bar{\Phi}$, respectively.

2- Back-propagation stage:

$$\bar{\Pi}(\bar{n}) = \bar{\mu}(\bar{n}) \cdot \bar{\Phi}\left[\bar{T}(\bar{n})\right] = \left[\bar{D}(\bar{n}) - \bar{O}(\bar{n})\right] \cdot \left[\bar{O}(\bar{n})\right] \cdot \left[1 - \bar{O}(\bar{n})\right], \tag{33}$$

where $\bar{O}$ and $\bar{D}$ are the actual and desired outputs, respectively. Also, $\bar{\Pi}$ is the local gradient function, and $\bar{\mu}$ illustrates the error function, respectively.

3- Weight values correction stage:

$$\bar{W}_{ab}(\bar{n}+1) = \bar{W}_{ab}(\bar{n}) + \Delta\bar{W}_{ab}(\bar{n}) = \bar{W}_{ab}(\bar{n}) + \bar{\tau}\,\bar{\Pi}(\bar{n}) \cdot \bar{O}(\bar{n}), \tag{34}$$

where $\bar{\tau}$ is the learning rate. Also, $\bar{W}_{ab}$ and $\bar{W}_{bc}$ are the weights between the input and hidden layers, and between the hidden and output layers, respectively.

C. Particle Swarm Optimization (PSO)

The PSO is an optimization method based on population inspired by social behavior of bird flocking or fish schooling developed by Eberhart and Kennedy [30]. The optimization procedure of PSO is initiated with a population of random solutions and searches for optima by updating generations. PSO has no evolution operators such as mutation and crossover in genetic algorithm; instead, potential solutions that named “particles” fly through the space of problem by following the current optimum particles. Each particle keeps track of its coordinates in the problem space which are associated with the best solution (best fitness) called "pbest” that it has achieved up to now. Another "best" value that is tracked by using PSO is the best value achieved so far by any particle in the particle neighbors. This parameter is "lbest". When a particle takes all the population as its topological neighbors, a global best is the best value which called "gbest". The PSO concept at any time stage consists of changing each particle’s velocity toward its "pbest" and "lbest" locations. Acceleration using a random term is weighted by separate random numbers being generated for acceleration toward "lbest" and "pbest" locations. A conceptual flowchart of PSO algorithm is illustrated in Fig. 4.

The numerical results of this work are presented separately in three following sections as: parametric analysis, prediction, and optimization.

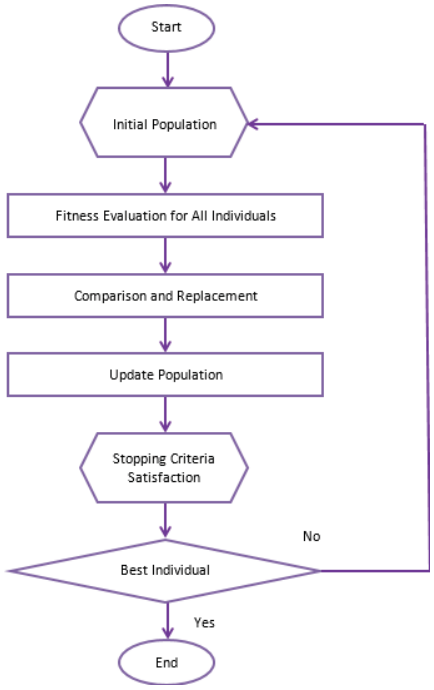

Fig. 4 A conceptual flowchart of PSO algorithm

V. Numerical Results

A. Parametric Analysis

In 3D MLPG problems, there are three degrees of freedom at the distributed nodes which are regularly or randomly distributed along all directions. These DOFs are in x, y and z directions which denotes as u_x, u_y, and u_z, respectively. Also, for obtaining the desired accuracy, the nodes can be added in each direction easily. Meanwhile, the number of gauss points is obtained based on a parametric analysis for

results accuracy maximization and finally assumed to be equal to 216 in the local sub-domain integration. In this study, the assumed boundary condition of the plate is simply supported edges, which can be defined as:

$$\sigma_x = 0, u_x = u_z = 0 \; on \begin{cases} x = 0 \\ x = a \end{cases}; \quad \sigma_y = 0, u_x = u_z = 0 \; on \begin{cases} y = 0 \\ y = b \end{cases} \tag{35}$$

The dimensionless sub-domain and support-domain sizes are described by ψ and τ, respectively. The values of these parameters are considered to be $\psi = 0.75$ and $\tau = 0.29$, which are obtained with investigation of accuracy of the results.

The obtained natural frequencies of MLPG method for simply supported square FG plate of this study is verified by comparing with those obtained by Qian et al. [22] for P=2 and h/a=0.2. The bottom layer in this study assumed to be zirconia with $E_{ZrO2} = 200\,GPa$ and $\rho_{ZrO2} = 5700\,kg/m^3$, and the top layer aluminum with $E_{Al} = 70\,GPa$ and $\rho_{Al} = 2707\,kg/m^3$. The number of nodes in each x, y, and z directions of the plate assumed to be 11 nodes. In this study, the natural frequency is presented in non-dimensional form as:

$$v = \omega . h \sqrt{\frac{\rho_m}{E_m}} \tag{36}$$

where $E_m = 70\,GPa$ and $\rho_m = 2702\,kg/m^3$.

The percentage of differences between the obtained data ($\overline{\omega}_P$) and results presented by Qian et al. [22] ($\overline{\omega}_Q$) is defined as error in the following form:

$$Error\,(\%) = \frac{(\overline{\omega}_P - \overline{\omega}_Q)}{\overline{\omega}_Q} \times 100 \tag{37}$$

In Table I, the errors of 1st to 5th natural frequencies are tabulated.

TABLE I
COMPARISON OF THE FIRST FIVE NON-DIMENSIONAL NATURAL FREQUENCIES OF THIS STUDY AND THAT OF QIAN ET AL. [22] FOR P=2 AND H/A=0.2

Parameter	ϖ_1	ϖ_2	ϖ_3	ϖ_4	ϖ_5
Present study	0.2177	0.4168	0.4175	0.4804	0.4817
Qian et al. [22]	0.2153	0.4034	0.4034	0.4720	0.4720
Error (%)	1.1436	3.3411	3.5173	1.7842	2.0588

The maximum and minimum percentages of errors are 1.14% and 3.51%, respectively. Therefore, the presented results can be regarded as good and reliable results.

The effects of volume fraction index of power-law FG model and also plate thickness to width ratios on non-dimensional natural frequencies are discussed using the MLPG analysis. Fig. 5 shows the effect of the volume fraction index on the first five non-dimensional natural frequencies of the FG plate for various values of thickness to width ratios.

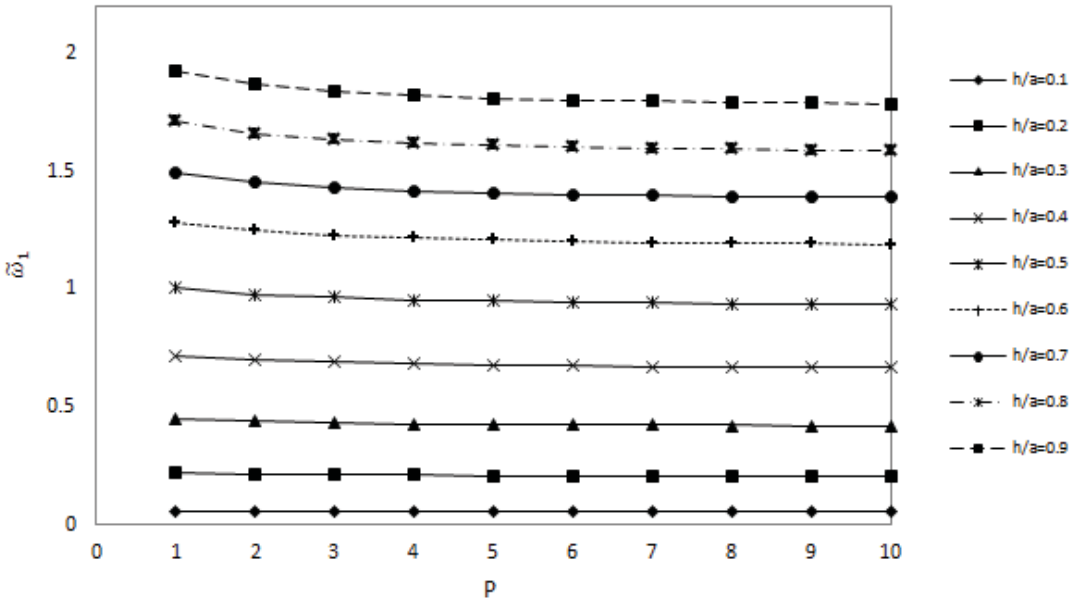

(A)

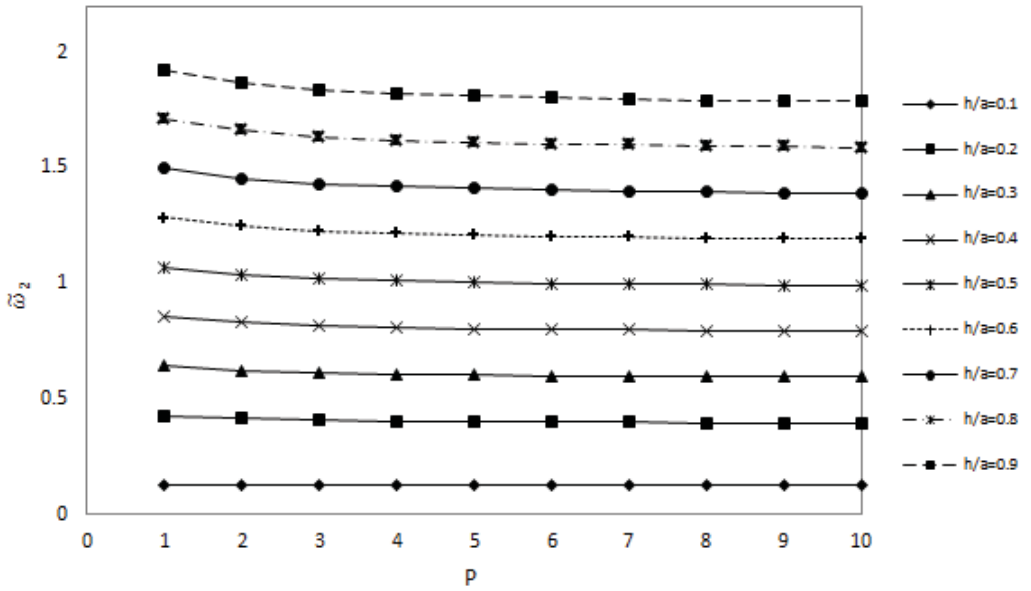
2
1.5
1
0.5
0
0
1
2
3
4
5
6
7
8
9
10
p
h/a=0.1
h/a=0.2
h/a=0.3
h/a=0.4
h/a=0.5
h/a=0.6
h/a=0.7
h/a=0.8
h/a=0.9

(B)

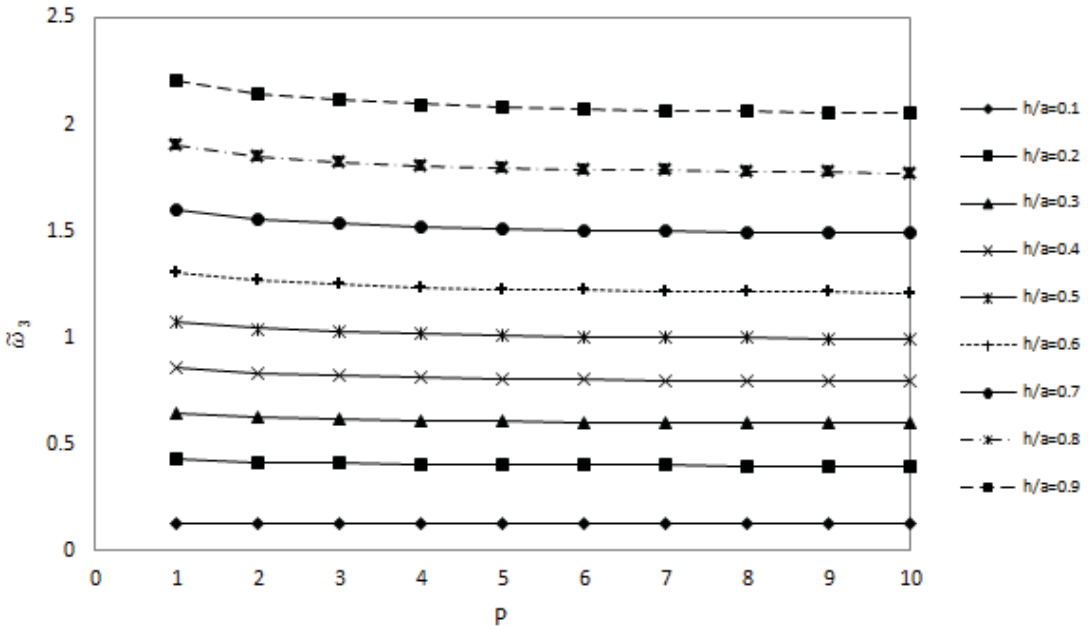
2.5
2
1.5
1
0.5
0
0
1
2
3
4
5
6
7
8
9
10
p
h/a=0.1
h/a=0.2
h/a=0.3
h/a=0.4
h/a=0.5
h/a=0.6
h/a=0.7
h/a=0.8
h/a=0.9

(C)

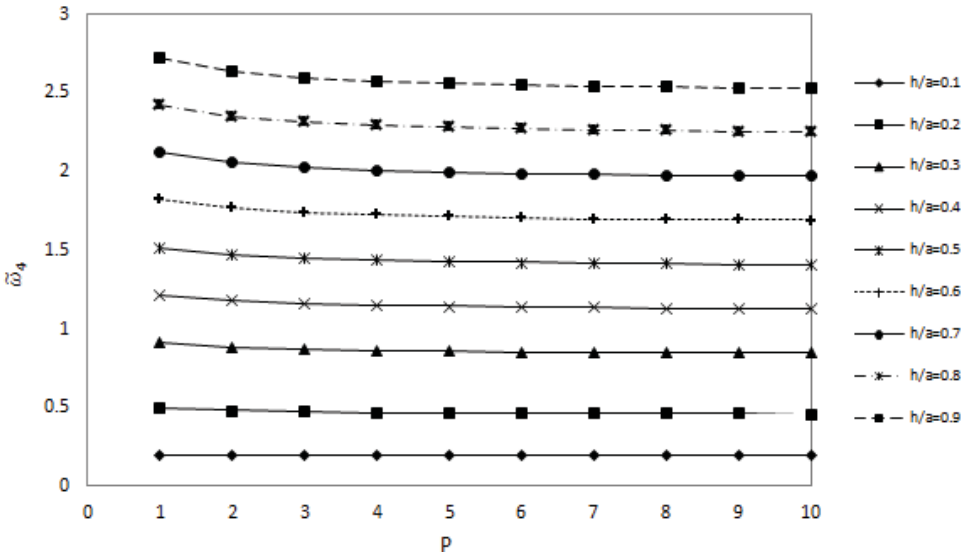

(D)

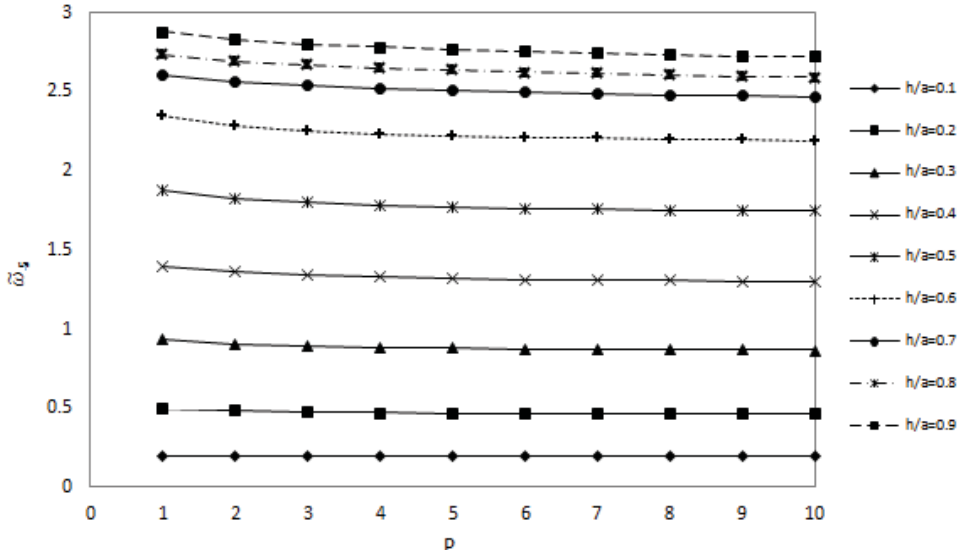

(E)

Fig. 5 Effect of volume fraction index on non-dimensional A) 1st B) 2nd C) 3rd D) 4th and E) 5th natural frequencies of the FG Plate for different thickness to width ratios (MLPG Results)

In Fig. 5, it can be seen that the curves have a slight decrease from $h/a=0.1$ to $h/a=1$ for all first five natural frequencies with respect to p. Also, it can be concluded that the graphs of bigger h/a values are upper than smaller ones. So, it is found that increasing h/a values leads to increasing of natural frequencies. Also, the absolute value of the curve's slop is decreased by increasing the value of p.

B. Prediction

In this part of study, a combination of MLPG method and ANN is employed to predict the non-dimensional first natural frequency of FG plate. MATLAB commercial software [31] is used to apply the ANN.

First of all, a MLFF neural network is created with one input, hidden and output layers. In the designed ANN, $N_I=2, N_H=20$ and $N_O=1$. The inputs of the ANN are h/a and p, and the target output is a non-dimensional first natural frequency. In the next step, the ANN is trained based on the data of 96 different conditions of FG plate, using the BEP method. BEP training trends are shown in Fig. 6. In the considered BEP training progress, 70%, 20%, and 10% of MLPG data are used for training, testing and verification, respectively.

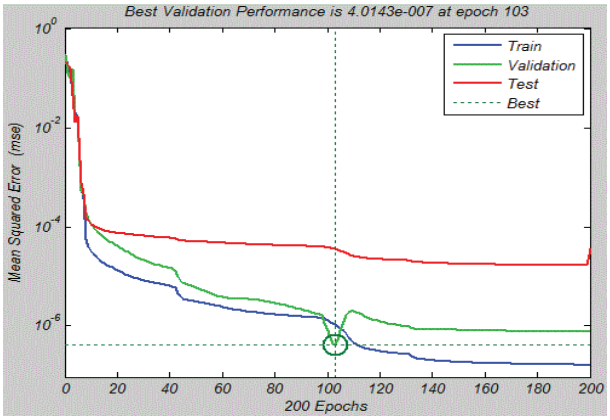

Fig. 6 BEP training trends

As can be seen the training error is less than 10^{-6}. In the training process of ANN, the BEP iterations are assumed to be 200. Although prediction results would be affected by taking other values for BEP constants, but it is not a concern of this study.

The BEP-based trained ANNs are tested for four other conditions of the FG plate which have not been used in the training procedure. The obtained results are compared with MLPG results and are tabulated in Table II.

TABLE II
ANN PREDICTED RESULTS VERIFICATION

Case No.	h/a	p	$\bar{\omega}_1$-MLPG	$\bar{\omega}_1$-ANN	Error (%)
1	0.3	6	0.425	0.427	0.25
2	0.5	4	0.955	0.956	0.01
3	0.6	5	1.209	1.210	0.025
4	0.7	7	1.399	1.401	0.09
Average					0.1

It can be found from Table II that the average error in prediction of first non-dimensional natural frequencies using proposed hybrid MLPG and ANN method is within 0.1%. Therefore, the predicted data have a good agreement with the actual data. It can be further concluded that the proposed method has a good capability of predicting the FG plate natural frequencies.

The predicted first non-dimensional natural frequencies for some other volume fraction index and plate thickness where MLPG results are not available are presented in Table III.

TABLE III
ANN-BASED NATURAL FREQUENCY PREDICTION

Case No	h/a	p	$\bar{\omega}_1$-ANN
1	0.35	0.55	0.549
2	0.45	0.75	0.809
3	0.67	0.42	1.365
4	0.54	0.85	1.043
5	0.65	0.4	1.329
6	0.8	0.35	1.625

C. Optimization

In this study, the PSO algorithm specifications are considered to be as follows: Population size = 10, Number of iterations = 20, Optimization variables = 2, The cost function is as (38):

$$CF = w_f f_{1n} - w_m m_n \tag{38}$$

where w_f and w_m are the weights of non-dimensional first natural frequency and non-dimensional total mass, respectively. Also f_{1n} and m_n are non-dimensional first natural frequency and non-dimensional total mass, respectively, which are defined as (39) and (40):

$$f_{1n} = f_1 / f^* \tag{39}$$

$$m_n = m / m^* \tag{40}$$

where f^* is the biggest value of 1st natural frequencies among 100 plates with different volume fraction index and plate thickness values. This maximum value belongs to plate with volume fraction index equal to 1 and plate thickness to width ratio equal to 1. This value in this study is 2.1365 (Hz). Also, m^* is the total mass of the plate with thickness to width ratio equal to 1 and the material of plate is purely zirconia. This value in this study is 5.7 × 106 kg. As stated in (41), the sum of weights of w_f and w_m is equal to 1.

$$w_f + m_n = 1 \tag{41}$$

For some different values of w_f and w_m, optimization is performed by using the PSO algorithm, and the results are presented in Table IV.

TABLE IV
OPTIMIZATION RESULTS OBTAINED FROM PSO ALGORITHM

w_f	w_m	p	h/a	CF
1	0	1	1	0.975
0.9	0.1	1.524	1	0.805
0.8	0.2	2.665	1	0.643
0.7	0.3	6.771	1	0.492
0.6	0.4	9.404	1	0.345
0.5	0.5	10	1	0.200
0.4	0.6	10	1	0.055
0.35	0.65	10	0.637	-0.008
0.3	0.7	10	0.1	-0.028
0.2	0.8	10	0.1	-0.036
0.1	0.9	10	0.1	-0.044
0	1	10	0.1	-0.052

As can be seen in this table, for w_f between 0 to 0.5 (w_m between 0.5 to 1), the optimum value of p is 10. Also, for w_f between 0.4 to 1 (w_m between 0 to 0.6) the optimum value of h/a is 1. Furthermore, for w_f between 0 to 0.3 (w_m

between 0.7 to 1), the optimum value of h/a is 0.1.

The optimization trends of PSO algorithm for two considered weights pairs of mass and natural frequency are illustrated in Fig. 7. As can be seen, the cost function is increased in 20 iterations and converges to a constant optimum value. Also, it is seen that in the first 3 PSO iterations, the cost function values increase sharply and then converge to optimum values.

VI. Conclusion

In this study, natural frequencies of a rectangular FG plate have been obtained by using MLPG method. The effects of two parameters fraction index and thickness to width ratios on the plate natural frequencies have been investigated. Then, an ANN is trained based on MLPG results and used for natural frequency prediction in some other cases where MLPG results are not available. The PSO algorithm was utilized for simultaneous optimization of plate mass and natural frequency. The optimization results provide the designers with useful information for specifying the parameters of the desired FG plate. All novelties of this study can furnish a designer with some beneficial information about the FG plate natural frequency and mass which can be summarized as follows:

(A) Parametric analysis of rectangular thick FG plate natural frequencies using 3D MLPG methods.

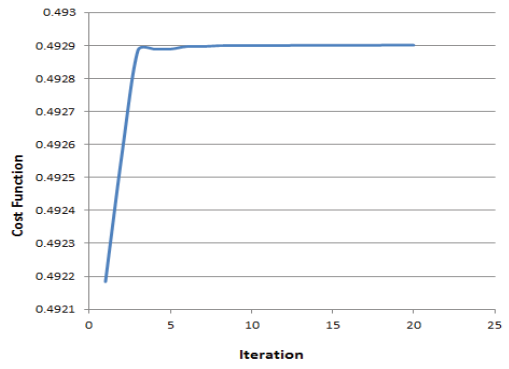

(a)

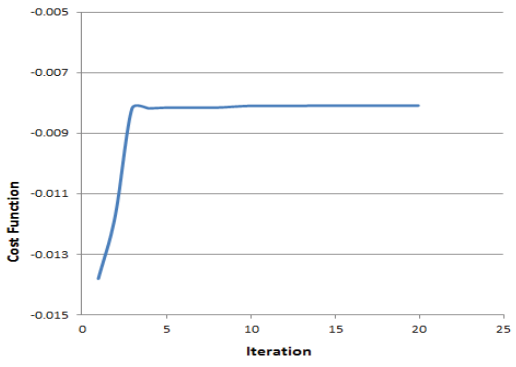

(b)

Fig. 7 The optimization trends of PSO algorithm for (a) , $w_f = 0.7 \& w_m = 0.3$ (b) $w_m = 0.35 \& w_m = 0.65$

(B) Prediction of the FG plate natural frequencies in some conditions where MLPG results were not available using ANN.

(C) Specifying the optimum values of parameters that concluded to maximum value for natural frequencies and minimum for mass by employing PSO and ANN.

References

[1] M. N. V. Ramesh, N. Mohan Rao", Free vibration analysis of pre-twisted rotating FGM beams", *Int J Mech Mater Des.,* vol. 9, no. 4, pp. 367–383, Oct. 2013.

[2] A. Safari Kahnaki, S.M. Hosseini, M. Tahani, "Thermal shock analysis and thermo-elastic stress waves in functionally graded thick hollow cylinders using analytical method", *Int J Mech Mater Des*., vol. 7, no. 9, pp. 167-184, Sep. 2011.

[3] A. Allahverdizadeh, M. H. Naei, A. Rastgoo Ghamsari, "The Effects of Large Vibration Amplitudes on the Stresses of Thin Circular Functionally Graded plates", *Int J Mech Mater Des*., vol. 3, no. 2, pp. 161-174, Jun. 2006.

[4] S. S. Vel, R.C. Batra", Three-dimensional exact solution for the vibration of functionally graded rectangular plates", *J Sound Vib.*, vol. 272, pp. 703-730, Jan. 2004.

[5] R. C. Batra, J. Jin", Natural frequencies of a functionally graded anisotropic rectangular plate", *J Sound Vib*, vol. 282, pp. 509-516, Jan. 2005.

[6] A. J. M. Ferreira, R. C. Batra, C. M. C. Roque, L. F. Qian, R. M. N. Jorge", Natural frequencies of functionally graded plates by a meshless method", *ComposStruct*., vol. 75, no. 1-4, pp. 593–600, Sep. 2006.

[7] C. M. C. Roque, A. J. M. Ferreira, R. M. N. Jorge", A radial basis function approach for the free vibration analysis of functionally graded plates using a refined theory", *J Sound Vib*., vol. 300, no. 3-5, pp. 1048–1070, March. 2007.

[8] H. Matsunaga", Free vibration and stability of functionally graded plates according to a 2-D higher-order deformation theory", *Compos Struct*., vol. 82, no. 4, pp. 499–512, Feb. 2008.

[9] Z. Iqbal, N. N. Muhammad, S. Nazra", Vibration characteristics of FGM circular cylindrical shells using wave propagation approach", *ActaMech.,* vol. 208, no. 3-4, pp. 237-248, Dec. 2009.

[10] S. M. Hosseini, M. H. Abolbashari", General analytical solution for elastic radial wave propagation and dynamic analysis of functionally graded thick hollow cylinders subjected to impact loading", *ActaMech*., vol. 212, no. 1, pp.1-19, June. 2010.

[11] M. Asgari, M. Akhlaghi, S.M. Hosseini", Dynamic analysis of two-dimensional functionally graded thick hollow cylinder with finite length under impact loading", *Acta Mech*., vol. 208, no. 3-4, pp. 163-180, Dec. 2009.

[12] M. M. Najafizadeh, M. R. Isvandzibaei", Vibration of functionally graded cylindrical shells based on higher order shear deformation plate theory with ring support", *ActaMech.,* vol. 191, no. 1, pp. 75-91, June. 2007.

[13] A. Fallah, M. M. Aghdam, M. H. Kargarnovin", Free vibration analysis of moderately thick functionally graded plates on elastic foundation using the extended Kantorovich method", *Arch. Appl. Mech*., vol. 83, no. 2, pp. 177-191, Feb. 2013.

[14] B. S. Aragh, M. H. Yas", Three-dimensional free vibration analysis of four-parameter continuous grading fiber reinforced cylindrical panels resting on Pasternak foundations", *Arch. Appl. Mech*. Vol. 81, no. 12, pp. 1759-1779, Dec. 2011.

[15] F. Ebrahimi, A. Rastgoo", Nonlinear vibration analysis of piezo-thermo-electrically actuated functionally graded circular plates", *Arch. Appl. Mech.,* vol. 81, no. 3, pp. 361-383, March. 2011.

[16] A. Allahverdizadeh, R. Oftadeh, M. J. Mahjoob, A. Soleimani, H. Tavassoli", Analyzing the effects of jump phenomenon in nonlinear vibration of thin circular functionally graded plates", *Arch. Appl. Mech*., vol. 82, no. 7, pp. 907-918, July. 2012.

[17] S. N. Atluri, T. A. Zhu, "A new meshless local Petrov–Galerkin (MLPG) approach in computational mechanics", *ComputMech*., vol. 22, no. 2, pp. 117-127, Aug. 1998.

[18] S. N. Atluri, H. G. Kim, J. Y. Cho, "A critical assessment of the truly meshless local Petrov–Galerkin (MLPG), and local boundary integral equation (LBIE) methods", *ComputMech*., vol. 24, no. 5, pp. 348–72, Nov. 1999.

[19] S. N. Atluri, T. Zhu, "Themeshless local Petrov–Galerkin (MLPG) approach for solving problems in elasto-statics", *Comput Mech*., vol. 25, no. 2, pp. 169–79, March. 2000.
[20] J. Sladek, P. Stanak, Z. D. Han, V. Sladek, S. N. Atluri", Applications of the MLPG Method in Engineering & Sciences: A Review", *Comput Model Eng Sci*., vol. 92, no. 5, pp. 423-475, 2013.
[21] J. Sladek, V. Sladek, C. H. Zhang", Stress analysis in anisotropic functionally graded materials by the MLPG method", *Eng Anal Bound Elem*., vol. 29, no. 6, pp. 597–609, June. 2005.
[22] L. F. Qian, R. C. Batra, L. M. Chena, "Static and dynamic deformations of thick functionally graded elastic plates by using higher-order shear and normal deformable plate theory and meshless local Petrov–Galerkinmethod", *Compos: Part B*., vol. 35, no. 6-8, pp. 685–97, Sep-Dec. 2004.
[23] D. F. Gilhooley, R. C. Batra, J. R. Xiao, M. A. McCarthy, J. W. Gillespie Jr", Analysis of thick functionally graded plates by using higher-order shear and normal deformable plate theory and MLPG method with radial basis functions", *ComposStruct*., vol. 80, no. 4, pp. 539–52, Oct. 2007.
[24] A. Rezaei Mojdehi, A. Darvizeh, A. Basti, H. Rajabi", Three dimensional static and dynamic analysis of thick functionally graded plates by the meshless local Petrov–Galerkin (MLPG) method", *Eng Anal Bound Elem*., vol. 35, no. 11, pp. 1168–1180, Nov. 2011.
[25] S. M. Hosseini, "Application of a hybrid meshless technique for natural frequencies analysis in functionally graded thick hollow cylinder subjected to suddenly thermal loading", *Appl Math Model*., vol. 38, no. 2, pp. 425-436, Jan. 2014.
[26] S. Kamarian, M. H. Yas, A. Pourasghar", Volume Fraction Optimization of Four-Parameter FGM Beams Resting on Elastic Foundation", *Int J Adv Des Manuf Tech.*, vol. 6, no. 4, pp. 75-82, 2013.
[27] A. Jodaei, M. Jalal, M. H. Yas", Free vibration analysis of functionally graded annular plates by state-space based differential quadrature method and comparative modeling by ANN", *Compos Part B*., vol. 43, no. 2, pp. 340-353, March. 2012.
[28] J. E. Jam, S. Kamarian, A. Pourasghar, J. Seidi", Free Vibrations of Three-Parameter Functionally Graded Plates Resting on Pasternak Foundations", *J Solid Mech*., vol. 4, no. 1, pp. 59-74.
[29] D. E. Rumelhart, J. L. McClelland, and PDP Research Group", Parallel distributed processing: Explorations in the microstructure of cognition", Vol. 1-2, 1986.
[30] J. Kennedy, R. Eberhart, "Particle Swarm Optimization". Proceedings of IEEE International Conference on Neural Networks, 1995, 1942–1948, Perth, Western Australia.
[31] MATLAB and Neural Network Toolbox Release 2010a, TheMathWorks, Inc., Natick, Massachusetts, United States.